DOI: 10.1002/chem.200801641

Aluminium Speciation in 1-Butyl-1-Methylpyrrolidinium Bis(trifluoromethylsulfonyl)amide/$AlCl_3$ Mixtures

Nathalie M. Rocher,*[a] Ekaterina I. Izgorodina,[a] Thomas Rüther,[b] Maria Forsyth,[a] Douglas R. MacFarlane,*[a] Theo Rodopoulos,[c] Michael D. Horne,[c] and Alan M. Bond[d]

Abstract: Electrodeposition of aluminium is possible from solutions of $AlCl_3$ dissolved in the 1-butyl-1-methylpyrrolidinium bis(trifluoromethylsulfonyl)amide ($C_4mpyrNTf_2$) ionic liquid. However, electrodeposition is dependant on the $AlCl_3$ concentration as it only occurs at concentrations $>1.6\,mol\,L^{-1}$. At these relatively high $AlCl_3$ concentrations the $C_4mpyrNTf_2/AlCl_3$ mixtures exhibit biphasic behaviour. Notably, at $1.6\,mol\,L^{-1}$ $AlCl_3$, aluminium can only be electrodeposited from the upper phase. Conversely, we found that at $3.3\,mol\,L^{-1}$ aluminium electrodeposition can only occur from the lower phase. The complex chemistry of the $C_4mpyrNTf_2/AlCl_3$ system is described and implications of aluminium speciation in several $C_4mpyrNTf_2/AlCl_3$ mixtures, as deduced from Raman and ^{27}Al NMR spectroscopic data, are discussed. The ^{27}Al NMR spectra of the $C_4mpyrNTf_2/AlCl_3$ mixtures revealed the presence of both tetrahedrally and octahedrally coordinated aluminium species. Raman spectroscopy revealed that the level of uncoordinated NTf_2^- anions decreased with increasing $AlCl_3$ concentration. Quantum chemical calculations using density functional and ab initio theory were employed to identify plausible aluminium-containing species and to calculate their vibrational frequencies, which in turn assisted the assignment of the observed Raman bands. The data indicate that the electroactive species involved are likely to be either $[AlCl_3(NTf_2)]^-$ or $[AlCl_2(NTf_2)_2]^-$.

Keywords: ab initio calculations · aluminum · electrodeposition · ionic liquids · NMR spectroscopy · Raman spectroscopy

Introduction

For several decades, ionic liquids have been widely investigated as electrolytes for the recovery of aluminium. Ionic liquids provide an alternative lower temperature, lower energy, approach to primary aluminium production than the traditional energy intensive Hall–Héroult industrial process. In the Hall–Héroult process, calcined alumina is electrolysed to aluminium metal in a molten bath of cryolite at 960 °C. Although aluminium electrodeposition has successfully been demonstrated from ionic liquids, the majority of the studies have been conducted using chloroaluminate ionic liquids[1–17] which are moisture sensitive and susceptible to decomposition.[18–20] Chloroaluminate ionic liquids are formed by mixing an organic halide with anhydrous $AlCl_3$, both of which are hygroscopic. Numerous studies on chloroaluminates have elucidated that the electrodeposition of aluminium is very dependent on the composition of the chloroaluminate.[21–25] Aluminium can only be electrodeposited from acidic chloroaluminates, that is, when the $AlCl_3$ mole fraction is greater than 0.5. Acidic chloroaluminates contain $Al_2Cl_7^-$, which is reducible within the electrochemical window of the chloroaluminate melt via the following reaction:

$$4\,Al_2Cl_7^- + 3e^- \rightleftharpoons Al + 7\,AlCl_4^-$$

Interest in ionic liquids as electrolytes for the recovery of re-

[a] Dr. N. M. Rocher, Dr. E. I. Izgorodina, Prof. M. Forsyth, Prof. D. R. MacFarlane
Australian Centre for Electromaterials Science
Monash University, Clayton, Victoria 3800 (Australia)
E-mail: d.macfarlane@sci.monash.edu.au

[b] Dr. T. Rüther
CSIRO Energy Technology and Light Metals Flagship
Box 312, Clayton South, Victoria 3169 (Australia)

[c] Dr. T. Rodopoulos, M. D. Horne
CSIRO Minerals and Light Metals Flagship, Box 312
Clayton South, Victoria, 3169 (Australia)

[d] Prof. A. M. Bond
Centre for Green Chemistry, Monash University
Clayton, Victoria 3800 (Australia)

Supporting information for this article is available on the WWW under http://dx.doi.org/10.1002/chem.200801641.

active metals such as aluminium increased after the discovery of air and water stable ionic liquids by Wilkes and Zaworotko.[26] This particular generation of ionic liquids has distinct advantages over chloroaluminates in electrochemical applications, such as ease of handling and drying. In 2004 Brausch et al.[27] reported the high solubility of $AlCl_3$ in water stable ionic liquids of the form [cation][NTf_2], where the cation is a pyridinium or imidazolium heterocycle and NTf_2 is the bis(trifluoromethylsulfonyl)amide anion. It was suggested that these highly acidic ionic liquid systems may be applicable to aluminium electroplating. The presence of $AlCl_3$ related species renders the liquid mixture water sensitive to an extent; nonetheless, the prospect of $<100\,^{\circ}C$ operation makes these mixtures interesting from a practical point of view. Shortly thereafter Zein El Abedin et al.[28] described the electrodeposition of nanocrystalline aluminium from the air and water stable ionic liquid 1-butyl-1-methylpyrrolidinium bis(trifluoromethylsulfonyl)amide ($C_4mpyrNTf_2$; Figure 1) saturated with $AlCl_3$. Zein El Abedin et al.[29] subsequently reported the electrodeposition of aluminium from two additional NTf_2-based ionic liquids, namely, 1-ethyl-3-methylimidazolium bis(trifluoromethylsulfonyl)amide ($C_2mimNTf_2$) and trihexyltetradecylphosphonium bis(trifluoromethylsulfonyl)amide ($P_{6,6,6,14}NTf_2$), containing $AlCl_3$. More recently, aluminium electrodeposition was reported from a dicyanamide (DCA)-based water stable ionic liquid containing $AlCl_3$.[30] Although aluminium electrodeposition has now been demonstrated from several water stable ionic liquids containing two different anions, the mechanism by which this occurs is still not well understood.

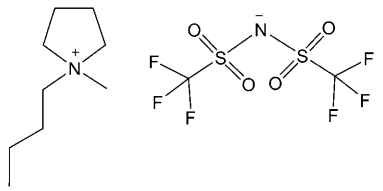

Figure 1. Structural formula of 1-butyl-1-methylpyrrolidinium bis(trifluoromethylsulfonyl) amide ($C_4mpyrNTf_2$).

Interestingly, Brausch et al.[27] noted that the [cation][NTf_2]/$AlCl_3$ mixtures exhibited cation and temperature dependent biphasic behaviour in certain composition ranges. Similar biphasic behaviour was witnessed by Zein El Abedin et al. in the $C_4mpyrNTf_2$/$AlCl_3$ system. Clear solutions were obtained for mixtures with an $AlCl_3$ concentration up to $1.5\,mol\,L^{-1}$ (i.e., moles of $AlCl_3$ in 1 L $C_4mpyrNTf_2$) from which aluminium could not be electrodeposited. At an $AlCl_3$ concentration between $1.6\,mol\,L^{-1}$ to just below $2.7\,mol\,L^{-1}$ the mixture becomes biphasic with a clear lower phase and a turbid white upper phase. Aluminium electrodeposits could only be obtained from the upper phase on gold and glassy carbon substrates at room temperature.[28] The biphasic mixtures become monophasic (a single clear phase) upon increasing the temperature to $80\,^{\circ}C$. As the $AlCl_3$ concentration was increased to $2.7\,mol\,L^{-1}$ the volume of the clear lower phase gradually decreased, eventually yielding a single solid white phase. It would appear that the aluminium speciation in $C_4mpyrNTf_2$ changes with increasing $AlCl_3$ concentration. Above a certain $AlCl_3$ concentration, an aluminium-containing species is generated in solution which is reducible to aluminium within the electrochemical window of $C_4mpyrNTf_2$. This reducible aluminium-containing species only exists in the upper phase of the biphasic mixtures. According to a ^1H, ^{13}C and ^{19}F NMR investigation of [*N*-butyl-4-methylpyridinium][NTf_2]/$AlCl_3$ biphasic mixtures Brausch et al.[27] suggested that the lower phase is formed by neutral, mixed chloro-NTf_2/aluminium species and the upper phase contains the *N*-butyl-4-methylpyridinium cation and a mixture of chloro-NTf_2/aluminate ions.

Clearly, aluminium speciation behaviour in the $C_4mpyrNTf_2$/$AlCl_3$ system is complex and the mechanism of aluminium electrodeposition is not yet understood. The objective of this work is to identify the aluminium species generated in the air and water stable $C_4mpyrNTf_2$ ionic liquid upon dissolution of anhydrous $AlCl_3$ and to identify the aluminium-containing species responsible for aluminium electrodeposition. A fundamental understanding of the aluminium deposition mechanism is critical if an industrial aluminium electrowinning or electroplating process using water stable ionic liquids is to be developed. In this study extensive Raman and ^{27}Al NMR spectroscopic investigations were carried out on $C_4mpyrNTf_2$/$AlCl_3$ mixtures as a function of composition. The spectroscopic studies were supported by ab initio calculations which aimed to identify plausible aluminium-containing species and assisted in the assignment of the Raman bands.

Experimental Section

Chemicals

1-Butyl-1-methylpyrrolidinium bis(trifluoromethylsulfonyl)amide (Merck, ultra pure; $C_4mpyrNTf_2$), 1-butyl-1-methylpyrrolidinium chloride (Merck; synthesis; $C_4mpyrCl$), anhydrous $AlCl_3$ (Aldrich, 99.999%), bistrifluoromethanesulfonimide (Fluka, >95%; $HNTf_2$) and triethylaluminium (Aldrich, 1.0 M in hexane) were used as received. Toluene (Merck, pro analysi) was freshly distilled from sodium prior to use. All chemicals were stored in an argon filled glove box and all manipulations were carried out in an argon filled dry box or a Schlenk line.

Instrumentation and analysis

The differential scanning calorimetry (DSC) measurements were performed on a TA Instruments Q100 calorimeter under a dry nitrogen flow of $50\,mL\,min^{-1}$ at heating and cooling rates of $10\,^{\circ}C\,min^{-1}$. An average sample weight of 10–15 mg was hermetically sealed in a 40 μL aluminum pan in an argon filled glove box. The thermograms were analyzed using Universal Analysis 2000 software from TA Instruments.

The ^{27}Al NMR spectra of the $C_4mpyrNTf_2$/$AlCl_3$, $C_4mpyrCl$/$AlCl_3$, and $C_4mpyrNTf_2$/$Al(NTf_2)_3$ mixtures were recorded with a Bruker Avance 300 spectrometer operating at 78.2 MHz. Samples were referenced to a very dilute solution of $AlCl_3$ in water. The solid-state and solution ($CDCl_3$) ^{27}Al and ^{19}F NMR spectra of the homoleptic $Al(NTf_2)_3$ complex were recorded with a Varian Unity Plus 300 spectrometer operating at

78.2 and 282.2 MHz, respectively. The ^{27}Al and ^{19}F chemical shift values were reported relative to an aqueous solution of $Al(NO_3)_3{\cdot}9H_2O$ and $CFCl_3$, respectively, as the external references.

FT-Raman spectra of $C_4mpyrNTf_2/AlCl_3$ mixtures and neat $Al(NTf_2)_3$ were recorded over the spectral range 100–1500 cm^{-1} using a Renishaw inVia Raman microscope in a backscattering geometry (180°). Samples were sealed in 5 mm Schott NMR tubes and illuminated with 514 nm radiation from a tunable Innova 70C argon/krypton laser with a laser power of 500 mW at the laser head and a 6% neutral density filter placed between the laser and the instrument. The spectra of $C_4mpyrNTf_2/AlCl_3$ mixtures containing high $AlCl_3$ concentrations were recorded with a Renishaw RM 2000 Ramascope equipped with a 782 nm diode laser with a laser power of 19 mW at the laser head, in a backscattering geometry (180°). An excitation wavelength of 782 nm allowed data collection with samples exhibiting fluorescence.

Positive and negative ion electrospray ionisation mass spectra were acquired on a VG Platform mass spectrometer using a cone voltage of 50 or 30 V and the source was maintained at 80 °C. The solvent system used was $CHCl_3$ with a flow rate of 0.04 mL min^{-1}. Electron impact (EI) mass spectra were acquired on a ThermoQuest MAT95XL mass spectrometer using an ionization energy of 70 eV. The solvent system used was $CHCl_3$.

Elemental analysis (C, H, N and F) was carried out by the Microanalytical Unit of the Research School of Chemistry at the Australian National University in Canberra.

Synthesis

$C_4mpyrNTf_2/AlCl_3$ mixtures: The $C_4mpyrNTf_2/AlCl_3$ samples of various compositions were prepared by simple addition of appropriate amounts of $AlCl_3$ to $C_4mpyrNTf_2$ in a glove box. The solutions were stirred for a minimum of 24 h before use. Samples which were biphasic or solids at room temperature were heated to 80 °C and stirred for approximately 40 min to ensure complete mixing. The different $C_4mpyrNTf_2/AlCl_3$ compositions prepared for this study are summarized in Table 1. In this work mole fractions in $AlCl_3$ (x_{AlCl_3}) were used as the concentration scale since it provides a direct insight into the stoichiometry of the mixture. Concentrations in moles of $AlCl_3$ per litre of $C_4mpyrNTf_2$ ionic liquid (note this is not the same quantity as molar = moles per litre of solution) were also calculated and listed in Table 1.

Table 1. Phase behaviour and aluminium electrochemistry of $C_4mpyrNTf_2/AlCl_3$ mixtures.

$AlCl_3$ mole fraction (x_{AlCl_3})	Mole ratio IL/$AlCl_3$	$AlCl_3$ [mol L^{-1}][a]	Phases[b]	Aluminium electrodeposition
0.05	20:1	0.17	clear solution	not possible
0.09	10:1	0.33		
0.17	5:1	0.67		
0.25	3:1	1.11		
0.33	2:1	1.67	biphasic; turbid upper layer, clear lower layer[c]	only from the turbid upper phase at RT
0.38	1.6:1	2.09		
0.43	1.3:1	2.57	white solid	possible above m.p.
0.45	1.2:1	2.78		
0.5	1:1	3.34	biphasic; hard solid on top, softer white solid at the bottom (≈equivalent volumes)	only from the lower phase above m.p.

[a] The $AlCl_3$ concentration here represents the number of moles of $AlCl_3$ in 1 litre of the $C_4mpyrNTf_2$ ionic liquid. [b] At room temperature. [c] Crystals form at the phase boundary.

$C_4mpyrAlCl_4$ chloroaluminate mixtures: $C_4mpyrCl/AlCl_3$ mixtures containing an $AlCl_3$ mole fraction of 0.25, 0.50 and 0.60 were prepared as reference samples by slow addition of appropriate amounts of $AlCl_3$ to $C_4mpyrCl$ with stirring in a glove box.

Homoleptic aluminium bis(trifluoromethylsulfonyl)amide complex [$Al_n(NTf_2)_{3n}$]: Although numerous examples of structurally characterised homoleptic metal bis(trifluoromethylsulfonyl)amide $[M_n(NTf_2)_m]$ complexes, where M = metal ion, have been reported,[31–35] there is yet no account of the synthesis and full characterisation of a homoleptic solvate free Al^{3+} complex with this versatile anion. The few reports on undefined "Al-NTf_2" products from the reaction between an Al^{3+} and a NTf_2^- precursor, often generated in situ, relate to their use as strong Lewis acids in organic transformations.[36–40]

The salt $[Al_n(NTf_2)_{3n}]$ is obtained under anhydrous conditions from the slow addition of three equivalents of the acidic form of bis(trifluoromethylsulfonyl)amide, $HNTf_2$, to a 1.0 M hexane solution of $Al(C_2H_5)_3$ at room temperature. Likewise, an almost identical product can be prepared by adding anhydrous $AlCl_3$ to a solution of $HNTf_2$ in toluene, thus avoiding the use of more difficult to handle pyrophoric Al/alyl compounds. In both cases, the products precipitated after a few minutes as white solids and in the case of $Al(C_2H_5)_3$ gas evolution (C_2H_6) is observed. The resultant salt is soluble or moderately soluble in polar solvents like chloroform, acetone, dimethoxyethane, tetrahydrofuran, methanol and acetonitrile. Some solubility was also observed in toluene and hexane, respectively. The salt hydrolyses readily upon exposure to air resulting in a clear oily liquid. The general composition of $[Al_n(NTf_2)_{3n}]$ was confirmed by microanalysis. Further characterisation was carried out by solid state and solution NMR as well as mass spectroscopy. The ^{27}Al solid state NMR of both products displays a single broad complex resonance which upon deconvolution can be resolved into three resonances in a ratio of 1:2.2:4.7 at δ −14, −15.8 and −17.8 ppm with the chemical shift values confirming octahedral symmetry for the chelated Al centre. Three slightly shifted resonances at −14.6, −16 and −17.4 ppm are also observed for a sample dissolved in chloroform (Figure 2a), however here the ratio of the three species is approaching 2:2:1. Numerous structural possibilities are typically observed in Al coordination compounds, among them mononuclear, multinuclear and mixed complex cation/complex anion combina-

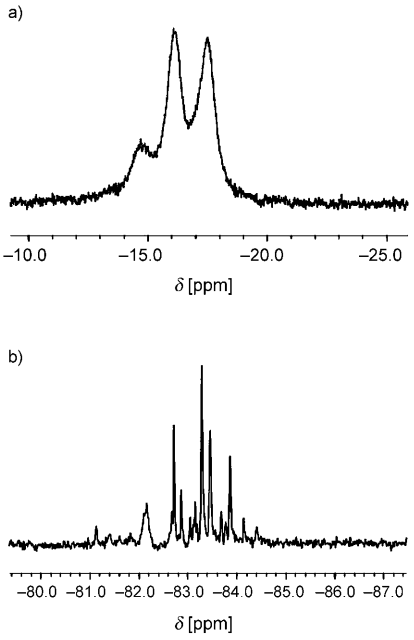

Figure 2. a) ^{27}Al and b) ^{19}F NMR spectrum of $Al(NTf_2)_3$ in $CDCl_3$ at 20 and 60 °C, respectively.

tions. In the simplest case of an octahedrally oxygen coordinated Al centre, four distinct isomers are feasible with the NTf_2 ligand. The free (uncoordinated) NTf_2^- anion can exist in two different conformations: a *transoid* arrangement with one CF_3 group above the S-N-S plane and the other below that plane or a *cisoid* arrangement where both CF_3 groups lie on the same side of the S-N-S plane. From computational studies it is clear that the *transoid* form is a few kJ mol^{-1} more stable in the free anion,[31,33,41] whereas in the majority of its metal chelates the anion displays a *cisoid* arrangement.[32] However, several examples of $[M_n(NTf_2)_m]$ complexes have been reported where *transoid* and *cisoid* anion arrangements coordinate the same metal centre.[34] Therefore the three isomers observed here are probably [Al(*trans*-$NTf_2)_3$], [Al(*cis*-$NTf_2)_3$] and [Al(*trans*-NTf_2)(*cis*-$NTf_2)_2$] or [Al(*cis*-NTf_2)(*trans*-$NTf_2)_2$]. Adding to the structural complexity is the fact that the *transoid* coordination mode turns the NTf_2^- into a disymmetric molecule. One *transoid* chelating ring exhibits a λ-configuration whereas one of the positions with mixed occupancy shows λ and δ-configurations.[34] This complexity in steric arrangements explains the myriad of peaks observed in the solution ^{19}F NMR spectrum of $[Al_n(NTf_2)_{3n}]$ (Figure 2b). After exposing the salt to moisture, one single resonance is observed in both the ^{27}Al and ^{19}F NMR solution spectra at δ 0.9 ppm and 85.4 ppm, respectively, the latter confirming the hydrolytic stability of the ligand.

$[Al_n(NTf_2)_{3n}]$ from $Al(C_2H_5)_3$: In a round bottomed flask equipped with a stir bar and a gas connection tap, a solution of $HNTf_2$ (1.54 g, 5.34 mmol) in freshly distilled toluene (5 mL) was slowly added to a 1.0 M solution of $Al(C_2H_5)_3$ in hexane (1.74 mL, 1.74 mmol). The reaction flask was immersed in an ethanol bath to quench any heat generated during the reaction. Strong gas evolution (vented to Schlenk line) was observed during the addition. A hazy mixture developed within minutes and a clear liquid separated which gradually solidified upon stirring at ambient temperature. After 1 h the supernatant was decanted, the remaining solid washed with toluene (3×2 mL) and the product dried under high vacuum at ambient temperature to yield an off-white solid (0.7 g, 46%). ^{27}Al NMR (solid state): $\delta = -14$ (s), -15.8 (s), -17.8 ppm (s); integration 1:2.2:4.7; ($CDCl_3$): $\delta = (14.6$ (s), -16 (s), -17.4 ppm (s); integration 1:2.2:2.3. ^{19}F NMR ($CDCl_3$): $\delta = -81$ to -85 ppm (multiplet); elemental analysis calcd (%) for: $C_6F_{18}N_3O_{12}S_6Al$: C 8.31, H 0.00, N 4.84, F 39.42; found: C 8.30, H 0.21, N 5.11, F 39.91; MS (+ESI, $CHCl_3$): *m*/*z* (%): 646 (100) $[Al_2(NTf_2)_2(OH)_2]^{2+}$, 987 (50) $[Al(NTf_2)_3(CHCl_3)H]^+$, 1190 (83) $[Al_2(NTf_2)_4(OH)]^+$, 1250 (32), 1328 (67), 1669 (32), 1812 (29); MS (EI, $CHCl_3$): *m*/*z* (%): 69 (100) $[CF_3^+]$, 586 (1.4) $[Al(NTf_2)_2]^+$.

$[Al_n(NTf_2)_{3n}]$ from $AlCl_3$: In a round bottomed flask equipped with a stir bar and a gas connection tap, neat $AlCl_3$ (0.192 g, 1.44 mmol) was added to a solution of $HNTf_2$ (1.24 g, 4.41 mmol) in freshly distilled toluene (4 mL). Gas evolution (HCl) was observed and the vessel was occasionally evacuated to remove HCl from the reaction equilibrium. The suspension became immediately bright yellow and this colour faded again within a few minutes while a clear liquid started to separate and gradually solidified upon stirring at ambient temperature. After 15 min the supernatant was decanted, the remaining solid washed with toluene (3× 2 mL) and the product dried under high vacuum at ambient temperature to yield an off-white solid (0.65 g, 49%). Elemental analysis calcd (%) for $C_6F_{18}N_3O_{12}S_6Al$: C 8.31, H 0.00, N 4.84, F 39.42; found: C 8.25, H 0.00, N 5.10, F 39.73.

Theoretical procedures: Standard ab initio molecular orbital theory calculations were carried out using the GAUSSIAN 03[42] set of programs. All geometry optimisations were performed using the B3LYP/6-31+G(d) method. All corrections for the zero-point vibrational energies were computed using scaled B3LYP/6-31G(d) frequencies.[43] Improved electronic energies were calculated using the B3LYP optimised geometries at a higher correlated level of theory, MP2/6-311+G(3df,2p). These total energies in conjunction with the scaled zero-point vibrational energies were used to calculate relative stabilities of the $[AlCl_3(NTf_2)]^-$ and $[AlCl_2(NTf_2)_2]^-$ anionic species with respect to various possible configurations. The optimised geometries, vibrational frequencies and Raman intensities of all the species studied here are given in the Supporting Information in the form of the GAUSSIAN archive files (see Table S4).

Results

Differential scanning calorimetry: The thermal analysis traces for the neat ionic liquid and selected $C_4mpyrNTf_2$/$AlCl_3$ mixtures are shown in Figure 3. The thermogram of neat $C_4mpyrNTf_2$ is complicated and shows three main regions: one glass transition (T_g) at −84 °C, a sharp exothermic crystallization transition (T_c) which starts at −52 °C, and a series of endothermic solid–solid and solid–liquid melt transitions (T_m). In the first run, the crystallization appears incomplete and finishes before the first solid-solid phase transition at −19 °C. The solid–liquid transition starts at −8 °C and does not satisfy Timmerman's criterion ($\Delta S_f < 20$ J K^{-1} mol^{-1}) for plastic crystal behaviour.[44] In the second run, however, crystallization is complete at −52 °C and three transitions are observed with onsets at −30, −18, and T_m at −7 °C. In this run, T_m satisfies Timmerman's criterion with an entropy of fusion of 7 J K^{-1} mol^{-1}. The difference between the two runs may arise from a metastable phase being formed in one of the runs (probably the first). When a small amount of $AlCl_3$ is added to yield a solution with $x_{AlCl_3} = 0.25$, the glass transition remains unchanged while a small crystallization is still observed, with onset at −31 °C, followed by a small melt starting at −7 °C. The measurements on this sample were repeated several times, with variation in the heating and cooling rates in order to obtain maximum crystallization. The transitions did not become more pronounced for this sample, which suggests that kinetics do not play an important role and that the phase changes are complete in all cases. Upon further addition of $AlCl_3$ such that $x_{AlCl_3} = 0.33$, new features appear in the thermogram that coincide with the appearance of a

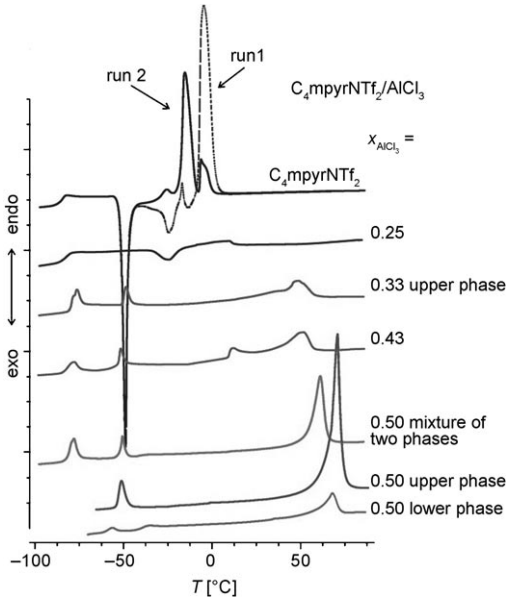

Figure 3. DSC thermograms of the pure ionic liquid and $C_4mpyrNTf_2$/$AlCl_3$ mixtures at $x_{AlCl_3} = 0.25$, 0.33, 0.43, and 0.50. For the biphasic sample $x_{AlCl_3} = 0.33$ sample, the thermogram shown corresponds to that of the upper turbid phase.

second, less dense phase, which seems to be composed of small crystals dispersed in a liquid phase. A sample of the turbid upper phase of the $x_{AlCl_3}=0.33$ composition was isolated; this shows two endothermic phase transitions with onsets at −50 and −80 °C, which are very close to the T_g and T_c values of the neat ionic liquid, an a very broad endothermic transition that commences around 0 °C, followed by a peak at 48 °C. The lower phase of this biphasic sample has a very similar thermogram to that of the $x_{AlCl_3}=0.25$ sample. As more $AlCl_3$ is added to form the monophasic solid sample at $x_{AlCl_3}=0.43$, the behaviour becomes similar to that of the turbid upper phase of the biphasic $x_{AlCl_3}=0.33$ sample, with the addition of a small well defined endothermic transition starting at 11 °C preceding the larger transition starting at 35 °C. The biphasic solid sample at $x_{AlCl_3}=0.50$ was separated into top and bottom phases. The hard and brittle top phase has a very large and sharp endothermic transition starting at 65 °C and peaking at 70 °C, which is also present in the bottom phase (softer solid) but with a much smaller intensity. It is also worth noting the difference in the lower temperature transitions between the two phases.

Optical microscope observations were made of the biphasic samples with $x_{AlCl_3}=0.33$–0.42 and are shown in the photographs in Figure 4. The samples have a turbid upper phase and a clear lower liquid phase. However, it seems that the upper phase is composed of small crystals dispersed in a clear liquid, which might be the same as the lower phase; in other words the sample is potentially a liquid–solid mixture in which the slightly less dense crystals have drifted towards the top of the sample. The samples, contained in an NMR tube, were observed using an optical microscope. The photographs reveal the majority of dispersed crystals in the upper phase are small and round in shape but closer to the lower liquid phase they appear to be snowflake-like (Figure 4a and b). Overnight, these snowflake-like crystals grow significantly to become fishbone-like crystals as shown in Figure 4c and d. This type of behaviour is typical of small crystals growing by an Ostwald ripening type mechanism in which diffusion limits the rate of growth and hence a dendritic (snow flake) pattern emerges. The melting point of this phase is too high for it to be the pure ionic liquid.

^{27}Al NMR spectroscopy: ^{27}Al NMR spectroscopy provides chemical shift data that can be used in probing coordination environment around the Al nucleus and therefore can provide valuable information regarding the aluminium-containing species generated in solution. The ^{27}Al chemical shifts generally move downfield when changing from six- to five- to four-coordinate aluminium. Chloroaluminate melts have been investigated by ^{27}Al NMR to ascertain the type and number of aluminium-containing species not engaged in rapid exchange in these melts at various compositions.[45–49] The resonances for the tetrahedral $AlCl_4^-$ and $Al_2Cl_7^-$ species were identified and the chemical shift difference between the two species was found to be quite small. Hence, in mixtures where $x_{AlCl_3}\approx 0.6$, the individual resonances of these two species are not fully resolved since chemical exchange between the species is evident.

The ^{27}Al NMR spectra of $C_4mpyrNTf_2/AlCl_3$ mixtures of various compositions were recorded and are shown in Figure 5. In general, a major resonance was observed at 103 ppm which is attributed to aluminium-containing species with tetrahedral coordination and a minor resonance was observed around −22 ppm which is attributed to aluminium-containing species with octahedral coordination. At $x_{AlCl_3}=$

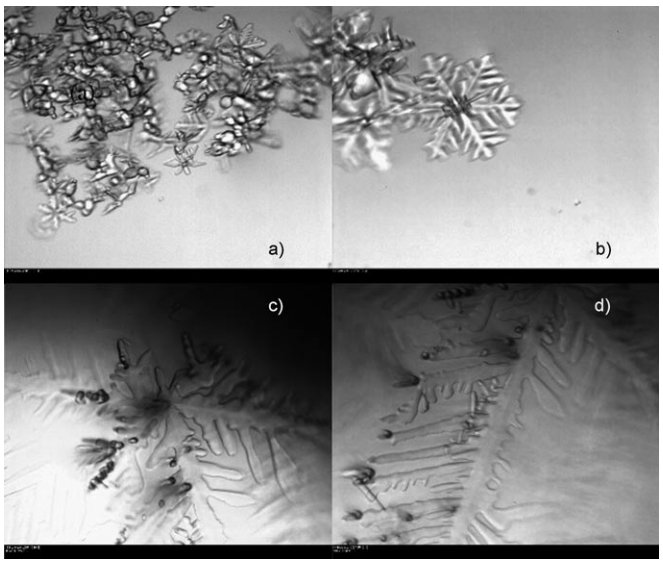

Figure 4. Photographs of an IL/$AlCl_3$ mixture at $x_{AlCl_3}=0.38$, taken with an optical microscope (magnification ×10) showing the various types of particles present at the interphase. Photos c) and d) were taken 24 h after a) and b).

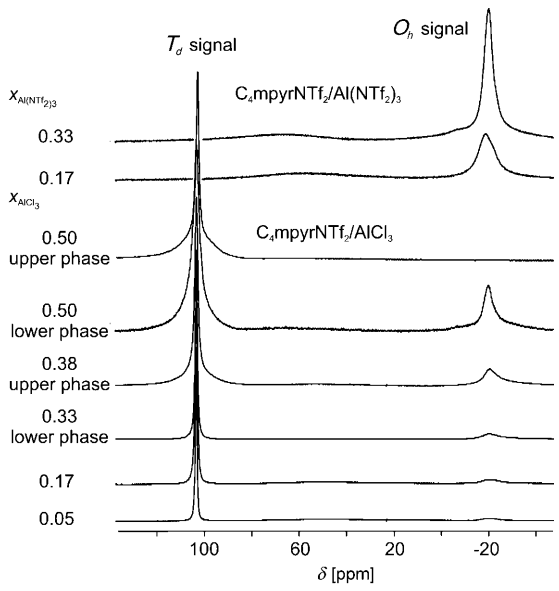

Figure 5. ^{27}Al NMR spectra of $C_4mpyrNTf_2/AlCl_3$ mixtures at various $AlCl_3$ mole fractions. The presence of two different Al coordination geometries (tetrahedral, T_d, and octahedral, O_h) are clearly visible. The two spectra at the top are the ^{27}Al NMR spectra of $C_4mpyrNTf_2/Al(NTf_2)_3$ mixtures at different $Al(NTf_2)_3$ mole fractions.

0.50, where the sample displays biphasic behaviour, the clear upper phase and turbid lower phase were isolated and their individual spectra were recorded. The spectrum of the lower phase exhibited resonances at both 103 and −22 ppm, while the upper phase only showed the single tetrahedral resonance at 103 ppm. It is important to recall that no aluminium electrodeposition could be obtained from the upper phase. This implies that the tetrahedral resonance observed at 103 ppm is not due to an electroactive Al-containing species.

Closer inspection of the upfield octahedral resonance at −22 ppm suggests that there are at least two octahedral aluminium-containing species present in mixtures with x_{AlCl_3} as low as 0.09. At $x_{AlCl_3}=0.17$, the octahedral resonance appears to be comprised of a main resonance at −21 ppm and a shoulder around −24 ppm. As x_{AlCl_3} increases the shoulder decreases in intensity leaving what appears to be a single octahedral resonance in the lower phase of the $x_{AlCl_3}=0.50$ sample. Line broadening of the tetrahedral peak was also observed as x_{AlCl_3} increased. This is attributed to an increase in viscosity which ultimately results in the solidification of the sample at room temperature when $x_{AlCl_3}=0.43$. An increased viscosity leads to longer molecular re-orientation correlation times. The effect is particularly noticeable in the turbid upper phase of the $x_{AlCl_3}=0.38$ sample and more so in the turbid lower phase of the $x_{AlCl_3}=0.50$ sample.

Examination of the tetrahedral resonance in the upper and lower phases of the $C_4mpyrNTf_2/AlCl_3$ system at $x_{AlCl_3}=0.50$ revealed that the linewidth in the upper phase was somewhat narrower than that in the lower phase. At 80 °C, where the samples are in the liquid state, the linewidth in the lower and upper phases was 30 and 15 Hz, respectively. At the same temperature, the chemical shift and linewidth of the tetrahedral resonance in the upper phase matched that of the $C_4mpyrCl/AlCl_3$ chloroaluminate system at $x_{AlCl_3}=0.50$ where $AlCl_4^-$ is the only aluminium-containing species present. This suggests that the upper phase of the $C_4mpyrNTf_2/AlCl_3$ system at $x_{AlCl_3}=0.50$ is likely to be the $C_4mpyrAlCl_4$ chloroaluminate. Further evidence supporting this conclusion is the fact aluminium could not be electrodeposited from this phase. It is well known that aluminium cannot be electrodeposited from $AlCl_4^-$ in chloroaluminate melts.[21–25]

The ^{27}Al NMR spectrum of the $C_4mpyrCl/AlCl_3$ chloroaluminate system at $x_{AlCl_3}=0.67$ was also recorded at 80 °C where the sample is in the liquid state and predominantly contains $Al_2Cl_7^-$ and smaller quantities of $AlCl_4^-$ and $Al_3Cl_{10}^-$. A single resonance at 103 ppm was observed with a linewidth (1400 Hz) significantly larger than that of the resonance in the $x_{AlCl_3}=0.50$ chloroaluminate sample. This is attributed to the presence of the bridged $Al_2Cl_7^-$ and $Al_3Cl_{10}^-$ species which have lower symmetry around the ^{27}Al nucleus than $AlCl_4^-$. The linewidth of this resonance is also significantly larger than that of the tetrahedral resonance obtained from the lower phase of the $C_4mpyrNTf_2/AlCl_3$ system at $x_{AlCl_3}=0.50$. Hence, it could be concluded that there are no bridged aluminium species analogous to $Al_2Cl_7^-$ and $Al_3Cl_{10}^-$. The tetrahedral resonance obtained from the lower phase is more than likely due to one or more species of the type $[AlCl_w(NTf_2)_y]^{z-}$. According to the narrow linewidth of 30 Hz for this resonance, the aluminium-containing species generating this resonance must be quite symmetric as it is well known that the linewidth of aluminium complexes decreases with increasing symmetry around the ^{27}Al nucleus. It is conceivable that $AlCl_4^-$ also contributes to the observed tetrahedral resonance, as its chemical shift is identical.

At low $AlCl_3$ concentrations in the $C_4mpyrNTf_2/AlCl_3$ system, it is plausible that NTf_2-rich aluminium species such as $Al(NTf_2)_3$ may be generated in solution due to the large excess of available NTf_2^- anions. Accordingly, the $C_4mpyrNTf_2/Al(NTf_2)_3$ system was examined in an effort to shed further light on the species formed in the $C_4mpyrNTf_2/AlCl_3$ mixtures. The ^{27}Al NMR spectra of the $C_4mpyrNTf_2/Al(NTf_2)_3$ system at an $Al(NTf_2)_3$ mole fraction ($x_{Al(NTf_2)_3}$) of 0.17 and 0.33 were collected and are also shown in Figure 5, top. A resonance at −20 ppm indicative of aluminium with octahedral symmetry was detected and, as expected, none of tetrahedral symmetry was evident. A weak shoulder at −23 ppm was also noticeable on the octahedral resonance in the spectra of the $x_{Al(NTf_2)_3}=0.17$ and 0.33 mixtures, indicating the presence of more than one octahedral aluminium-containing species. These are due to isomers of $Al(NTf_2)_3$ as the solution ^{27}Al NMR spectrum of $Al(NTf_2)_3$ also revealed the presence of several species (see Figure 2). The chemical shift of the $Al(NTf_2)_3$ octahedral resonances in Figures 2 and 5 is very similar to the octahedral resonances observed in the $C_4mpyrNTf_2/AlCl_3$ mixtures which suggests they are likely to be due to NTf_2-rich aluminium-containing species such as $Al(NTf_2)_3$ or perhaps $[AlCl_2(NTf_2)_2]^-$.

Raman spectroscopy and theoretical calculations: Raman spectroscopy has been shown to be useful in the study of NTf_2-based ionic liquids and metal salts.[50–58] The ionic association of the NTf_2^- anion can be monitored by analysing the shift of the strong Raman band around 740 cm^{-1}.[50–54] This band was originally attributed to the symmetric deformation of the CF_3 group, $\delta_s(CF_3)$, of a free NTf_2^- anion, however, it is now described as a complex mixture of internal coordinates such as $\nu_s(SNS)$, $\delta(SNS)$, $\delta(CF_3)$ and $\delta(SO_2)$ (with the major contribution from $\nu_s(SNS)$), which make the entire NTf_2^- anion expand and contract.[51,52] In this report we refer to this complex band as ν_{expand} for convenience. A vibration such as this will produce a large polarisability change and consequently an intense Raman band. This band will significantly be affected by changes in the coordination environment of the NTf_2^- anion. However, it has been shown that this particular mode is not sensitive to conformational isomerism hence it cannot be used to distinguish the *transoid* and *cisoid* conformers of the NTf_2^- anion.[51,56–58]

In Figure 6, the 700–800 cm^{-1} region of the Raman spectra of $C_4mpyrNTf_2/AlCl_3$ mixtures of various compositions are shown. It can be seen that the degree of ionic association of the NTf_2^- anion increased with increasing $AlCl_3$ con-

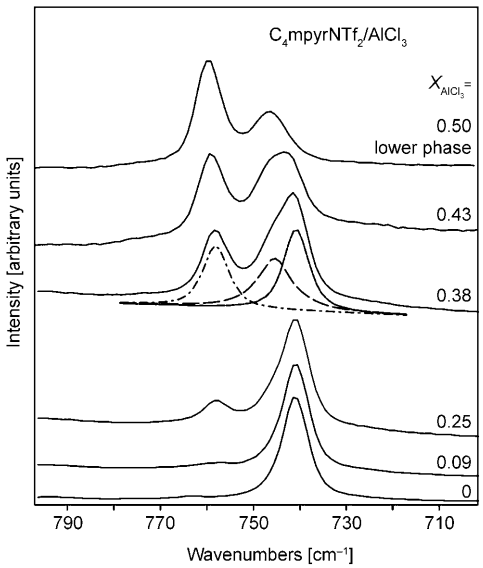

Figure 6. Raman spectra in the 700–800 cm^{-1} region of $C_4mpyrNTf_2/AlCl_3$ mixtures at various $AlCl_3$ mole fractions.

centration. In the pure $C_4mpyrNTf_2$ ionic liquid, a strong band at 741 cm^{-1} and a very weak band at 762 cm^{-1} were observed. The major vibrational frequency is assigned to ν_{expand} in the "free" NTf_2^- anion. Upon $AlCl_3$ addition to the $C_4mpyrNTf_2$ ionic liquid, two higher frequency bands start to grow at 746 and 758 cm^{-1}, which are assigned to ν_{expand} in the "Al^{3+}-coordinated" NTf_2^- anion. The higher frequency band at 758 cm^{-1} is evident at $x_{AlCl_3}=0.09$ whereas the band at 746 cm^{-1} becomes apparent at $x_{AlCl_3}=0.38$. The bands in the 700–800 cm^{-1} region of the spectrum were deconvoluted and the resolved spectra from the curve fitting analysis are shown in Figure 6 for the $x_{AlCl_3}=0.38$ sample. At this composition the sample is biphasic, and surprisingly the turbid upper phase and the clear lower phase display identical bands in this region of the spectrum, which means that the ionic association of the NTf_2^- anion is similar in both phases. The results of the curve fitting analysis for the $C_4mpyrNTf_2/AlCl_3$ mixtures of various compositions are shown in Table 2. The spectrum of the lower phase of the $x_{AlCl_3}=0.50$ sample does not exhibit a band indicative of "free" NTf_2^-, but has two bands indicative of "Al^{3+} coordinated" NTf_2^-. Similarly there is no band indicative of "free" NTf_2^- in the spectrum of the upper phase of the $x_{AlCl_3}=0.50$ sample, but in contrast the intensity of the bands indicative of "Al^{3+} coordinated" NTf_2^- are very weak, almost insignificant, suggesting the absence of NTf_2^- anion from this upper phase. A more detailed analysis of this upper phase is provided later.

Table 2. Results from the curve fitting analysis of the NTf_2 expanding band, ν_{expand}, in the 700 to 800 cm^{-1} region of the Raman spectra of $C_4mpyrNTf_2/AlCl_3$ mixtures of various compositions.

$AlCl_3$ mole fraction (x_{AlCl_3})	Proportion of each species [%]		
	"Al^{3+}-coordinated" NTf_2^-		"Free" NTf_2^-
	758–760 cm^{-1}	746–747 cm^{-1}	741–742 cm^{-1}
0	0	0	100
0.03	0	3	97
0.09	2	10	88
0.25	15	18	67
0.38 (both phases)	27	36	37
0.43	32	44	24
0.50 (lower phase)	59	41	0
0.50 (upper phase)	very small	very small	0

DFT calculations carried out on the more stable *transoid* NTf_2^- conformer (which has C_2 symmetry), suggest that the ν_{expand} mode should be located at 701 cm^{-1} and have a strong Raman intensity. The B3LYP/6-31+G(d) method underestimates this mode by almost 40 cm^{-1}. Although a similar discrepancy between theoretical and experimental vibrational frequencies was previously noted for the ν_{expand} mode, this computational method has been shown to provide quite realistic molecular geometries and vibrational frequencies for the NTf_2^- anion.[51,52] In the theoretical calculations, two modes assigned mainly to the symmetric deformation of CF_3, $\delta_s(CF_3)$, appear at 738 and 750 cm^{-1}. Of these, only the band at 750 cm^{-1} is Raman active and can yield a band of low intensity. The theoretically calculated band at 750 cm^{-1} is in good agreement (within 1%) with the experimentally observed peak at 762 cm^{-1} of very low intensity. It is well known in the literature that DFT (including B3LYP/6-31+G(d)) and lower levels of ab initio theory usually underestimate the frequency of symmetric stretching vibrations of highly symmetric species. For example, the theoretical frequency of the totally symmetric stretching vibration of the perchlorate anion (ClO_4^-) is always lower than that experimentally observed.[59] The same situation occurs for the totally symmetric stretching vibration of the tetrahedral chloroaluminate $AlCl_4^-$, for which theory underestimates the experimental data by 4.5%.[60] Therefore, following the approach of Scott et al,[43] in the discussion below, the calculated Raman frequencies of the ν_{expand} mode were multiplied by a factor of 1.057. The calculated bending and deformation vibrations are normally in good agreement with measured spectra hence scaling of these vibrational modes is not needed.

In the absence of more coordinating ligands, NTf_2^- can be considered a weakly coordinating ligand due to its delocalised negative charge. In principle, it can complex a metal ion via four coordination modes. The NTf_2^- anion will adopt the coordination mode which best accommodates the electronic and steric preference of the metal ion. It can behave as a monodentate ligand coordinating a metal ion directly through either a N or O atom or it can behave as a bidentate ligand coordinating the metal ion via O,O or O,N atoms and forming stable six-membered chelate rings. In order to assign the ν_{expand} modes observed at 746–747 cm^{-1} and 758–760 cm^{-1} to different coordination modes of the NTf_2^- anion, the Raman spectra of $[AlCl_3(NTf_2)]^-$ and $[AlCl_2(NTf_2)_2]^-$ were calculated. These two particular species were chosen as they are good examples of plausible tetrahedral and octahedral aluminium complexes containing both of the available anions (NTf_2^- and Cl^-) in the mixtures. The spec-

tra of $[AlCl(NTf_2)_3]^-$ were also studied theoretically (for more detail refer to the Supporting Information: Figure S2 and Tables S2–S4). According to DFT optimisations, only two configurations of tetrahedral geometry are possible for $[AlCl_3(NTf_2)]^-$ (Figure 7a) where the NTf_2^- anion behaves as a monodentate ligand coordinating aluminium via a single N atom (structure **1a**) or a single O atom (structure **1b**). In energy terms, the configurations are practically indistinguishable (only 9 kJ mol^{-1} separates the two species). Configurations with a higher coordination number are not feasible for this particular species, as attempts to optimise species with a coordination number of 5 (i.e., NTf_2^- anion behaving as a bidentate ligand) resulted in convergence back to tetrahedral structures.

A different situation is observed for the $[AlCl_2(NTf_2)_2]^-$ species where the energy difference between the possible configurations is more pronounced in comparison to the $[AlCl_3(NTf_2)]^-$ species. All possible configurations obtained from the DFT optimisations are presented in Figure 7b. It can be seen from these configurations that the coordination of the NTf_2^- anion has a direct impact on the geometry of the resultant aluminium complex. When it coordinates aluminium in a monodentate manner via a single N or O atom it results in tetrahedral geometries (structures **2**, **3** and **5** in Figure 7b). However, when it coordinates aluminium in a bidentate manner via O,O or N,O atoms it results in octahedral geometries (structures **4**, **6** and **7** in Figure 7b). Of the six possible $[AlCl_2(NTf_2)_2]^-$ configurations, octahedral structure **6**, where both NTf_2^- ligands are coordinated via O,O atoms, is 20 kJ mol^{-1} more stable than structure **7**, where one NTf_2^- ligand is coordinated via O,O atoms and the other via N,O atoms, and >40 kJ mol^{-1} more stable than the rest. When the aluminium complex becomes NTf_2-rich (i.e., more than one NTf_2^- ligand per aluminium centre) the geometric preference of the aluminium appears to be octahedral. This is illustrated by the $Al(NTf_2)_3$ complex where the asymmetric unit of the crystal structure[61] shows Al^{3+} coordinated by three NTf_2^- anions via their O atoms (O,O coordination).

From the calculated vibrational frequencies and their Raman intensities (see Supporting Information, Table S1), it is more likely that the strong band experimentally recorded at 760 cm^{-1} originates from the ν_{expand} mode of the NTf_2^- anion coordinated via O,O atoms as seen in structures **6** and **7**. This finding was supported by DFT calculations on the homoleptic $Al(NTf_2)_3$ complex shown in Figure 7c that is found to be of the lowest energy. Additional $Al(NTf_2)_3$ structures considered are included in Supporting Information, Figure S1. Theoretical calculations predict two bands corresponding to the ν_{expand} mode at 764 and 767 cm^{-1}, with the triple degenerate $\delta_s(CF_3)$ mode occurring at 756–757 cm^{-1}. The latter is likely to be overshadowed by the other two stronger bands at higher wavenumbers. On the other hand, the mode at 746–747 cm^{-1} appears to originate from NTf_2^- anions that are coordinated via a N atom, be it monodentate or bidentate (N,O). However, the $\delta_s(CF_3)$ mode is the main contributor to the observed band, as opposed to the ν_{expand} mode which is a mixture of $\nu_s(SNS)$, $\delta(CF_3)$, δ-(SNS), and $\delta(SO_2)$.

The Raman spectra of pure $Al(NTf_2)_3$ and $C_4mpyrNTf_2$/$Al(NTf_2)_3$ mixtures were also recorded to assist the assignment of the bands observed in the $C_4mpyrNTf_2/AlCl_3$ mixtures. In Figure 8 the 700–800 cm^{-1} region of the Raman spectra of pure $Al(NTf_2)_3$ and $C_4mpyrNTf_2/Al(NTf_2)_3$ mixtures at $x_{Al(NTf_2)_3}=0.17$ and 0.33 are presented. Only one band at 760 cm^{-1} is observed for pure $Al(NTf_2)_3$, which according to the theoretical calculations and the crystal structure[62] is indicative of O,O bidentate coordination of all three NTf_2^- ligands.

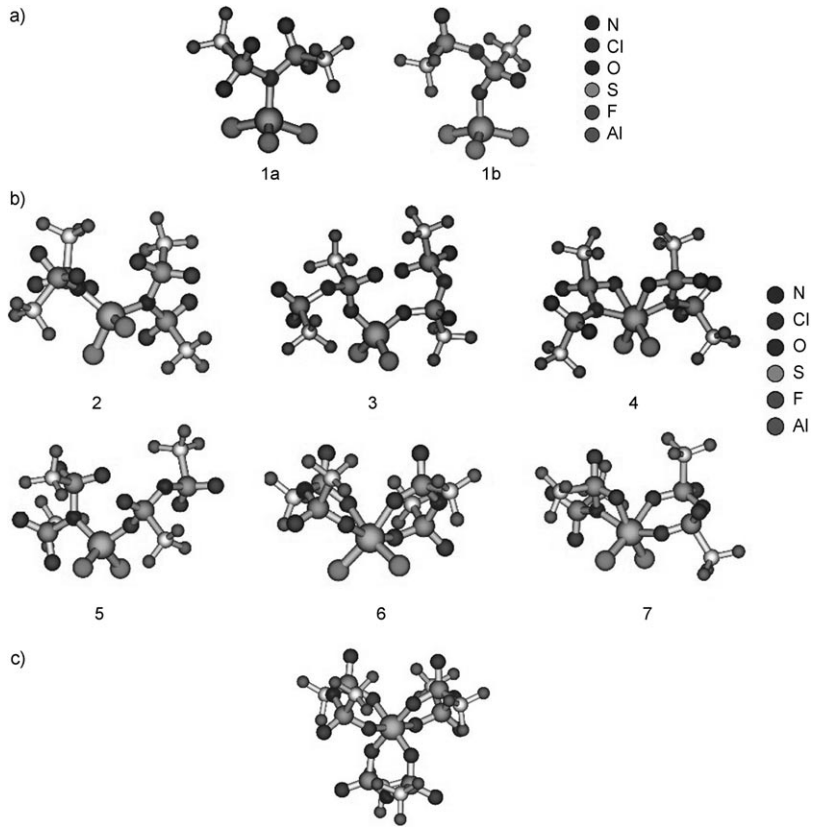

Figure 7. a) Optimised structures of the tetrahedral $[AlCl_3(NTf_2)]^-$ anions. b) Optimised structures of the tetrahedral and octahedral $[AlCl_2(NTf_2)_2]^-$ anions. c) Optimised structure of the octahedral $Al(NTf_2)_3$.

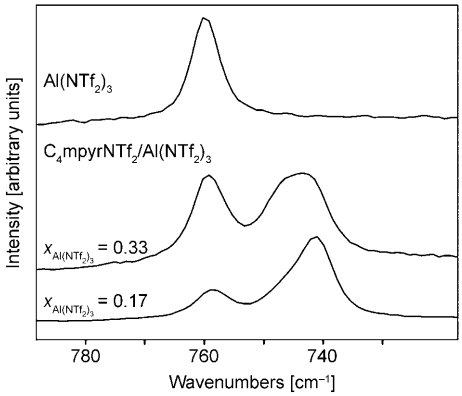

Figure 8. Raman spectra in the 700–800 cm^{-1} region of pure $Al(NTf_2)_3$ and $C_4mpyrNTf_2/Al(NTf_2)_3$ mixtures at $x_{Al(NTf_2)_3}=0.17$ and 0.33.

The spectrum of the $C_4mpyrNTf_2/Al(NTf_2)_3$ mixture at $x_{Al(NTf_2)_3}=0.17$ reveals two bands at 759 and 742 cm^{-1}. Increasing the $Al(NTf_2)_3$ concentration such that $x_{Al(NTf_2)_3}=0.33$ results in an increase in intensity of the band at 759 cm^{-1} relative to that at lower wavenumber. From the spectrum at $x_{Al(NTf_2)_3}=0.33$ it can clearly be seen that the band at lower wavenumber and centred around 745 cm^{-1} is a mixture of modes. Deconvolution of this NTf_2^- band indicates it is comprised of modes at 747 and 742 cm^{-1}. Hence, bands assigned to both "Al^{3+} coordinated" NTf_2^- anions (747 and 759 cm^{-1} modes) and "free" NTf_2^- anion (742 cm^{-1} mode) are present in the $C_4mpyrNTf_2/Al(NTf_2)_3$ samples. Comparison of these spectra to those of the $C_4mpyrNTf_2/AlCl_3$ mixtures (Figure 6) suggests the coordination environment of the NTf_2^- anion is similar in both systems.

The low frequency region (400–150 cm^{-1}) of the Raman spectra of $C_4mpyrNTf_2/AlCl_3$ mixtures of various compositions are shown in Figure 9. This region is devoid of any cation vibrational modes and has been shown to display distinct features arising from the *cisoid* and *transoid* conformers of the NTf_2^- anion.[51,56] Upon addition of $AlCl_3$ up to $x_{AlCl_3}=0.50$, the features originating from the NTf_2^- conformation bands become smaller and four bands at 347, 264, 259 and 179 cm^{-1} grow. The spectra eventually become dominated by the band at 347 cm^{-1}. At higher $AlCl_3$ concentrations, another band at 306 cm^{-1} grew between two of the NTf_2^- conformation bands. This band is evident in the spectra of the $x_{AlCl_3}=0.43$ sample and in the lower phase of the $x_{AlCl_3}=0.50$ sample. The modes around 260 and 300 cm^{-1} are assigned to a mixture of $\rho(CF_3)$ and $\rho(SO_2)$ modes and are present in all of the calculated structures (**1a** to **7**). Hence, these bands cannot be used to assign specific NTf_2^- coordination modes. Interestingly, the conformational NTf_2^- bands at 264 and 259 cm^{-1} are absent in the spectrum of the upper phase of the $x_{AlCl_3}=0.50$ sample (see Figure 10), while the 347 and the 179 cm^{-1} bands are still very strong.

To glean insights into the nature of the five bands present at 347, 306, 264, 259 and 179 cm^{-1} in the $C_4mpyrNTf_2/AlCl_3$ mixtures, the Raman spectra of three $C_4mpyrCl/AlCl_3$ chloroaluminate melts at $x_{AlCl_3}=0.25$, 0.50, and 0.60 were recorded. The low frequency region of their spectra are presented in Figure 10 along with that of pure $Al(NTf_2)_3$, $C_4mpyrNTf_2/Al(NTf_2)_3$ mixture at $x_{AlCl_3}=0.33$, and the upper and lower phases of $C_4mpyrNTf_2/AlCl_3$ at $x_{AlCl_3}=0.50$. The dependence of the relative proportion of the various chloroaluminate

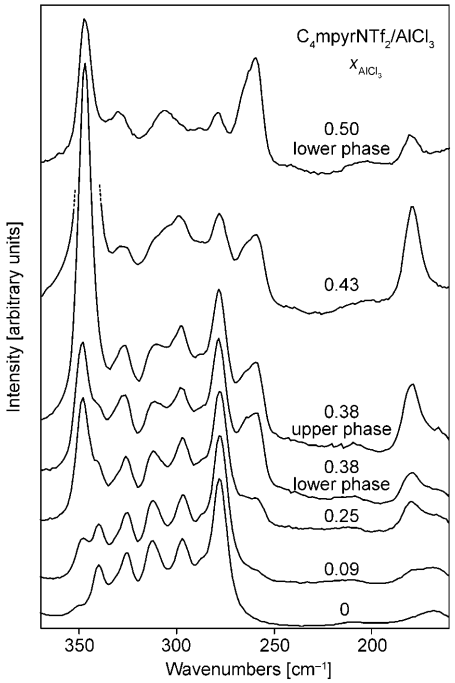

Figure 9. Raman spectra in the 150–400 cm^{-1} region of $C_4mpyrNTf_2/AlCl_3$ mixtures at various $AlCl_3$ mole fractions.

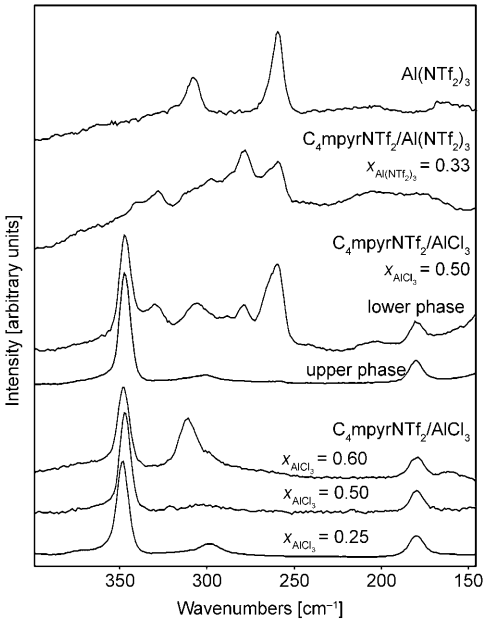

Figure 10. Raman spectra in the 150–400 cm^{-1} region of pure $Al(NTf_2)_3$, $C_4mpyrNTf_2/Al(NTf_2)_3$ at $x_{Al(NTf_2)_3}=0.33$, $C_4mpyrNTf_2/AlCl_3$ at $x_{AlCl_3}=0.50$ (upper and lower phase), and $C_4mpyrCl/AlCl_3$ chloroaluminate mixtures at $x_{AlCl_3}=0.25$, 0.50 and 0.60.

species as a function of x_{AlCl_3} in chloroaluminate ionic liquids is known.[62] Consequently, three C_4mpyrCl/$AlCl_3$ chloroaluminate melts at $x_{AlCl_3}=0.25$, 0.50, and 0.60 were specifically prepared in order to yield samples which contained Cl^- and $AlCl_4^-$, only $AlCl_4^-$, and an equimolar mixture of $AlCl_4^-$ and $Al_2Cl_7^-$, respectively. According to the spectra of the C_4mpyrCl/$AlCl_3$ chloroaluminate melts, the two bands at 347 and 179 cm^{-1} are indicative of $AlCl_4^-$ whilst the two bands at 433 and 311 cm^{-1} are indicative of $Al_2Cl_7^-$. These bands matched those previously recorded for these species.[63–65] The bands for $Al_2Cl_7^-$ were absent in the spectra of the upper and lower phases of C_4mpyrNTf$_2$/$AlCl_3$ at $x_{AlCl_3}=0.50$ confirming $Al_2Cl_7^-$ was not responsible for aluminium electrodeposition from the lower phase. Surprisingly the spectrum of the upper phase was virtually indistinguishable from that of the C_4mpyrCl/$AlCl_3$ chloroaluminate melt at $x_{AlCl_3}=0.50$ (Figure 11). Hence, the upper phase of C_4mpyrNTf$_2$/$AlCl_3$ at $x_{AlCl_3}=0.50$ is more than likely [C_4mpyr][$AlCl_4$], and explains why aluminium could not be electrodeposited from this phase.

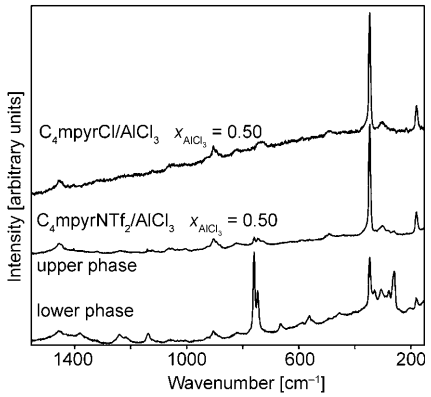

Figure 11. Raman spectra of the upper and lower phases of the C_4mpyrNTf$_2$/$AlCl_3$ mixture at $x_{AlCl_3}=0.50$ as well as the C_4mpyrCl/$AlCl_3$ chloroaluminate mixture at $x_{AlCl_3}=0.50$.

The Raman spectrum of the separated turbid upper phase of the C_4mpyrNTf$_2$/$AlCl_3$ sample at $x_{AlCl_3}=0.38$ sample revealed that the 347 cm^{-1} and the 179 cm^{-1} bands were much stronger than the other bands which suggests the presence of $AlCl_4^-$. However, this was the phase from which Zein El Abedin et al.[28] demonstrated aluminium electrodeposition. Therefore it is possible that the fine solid suspended in the turbid upper phase of the $x_{AlCl_3}=0.38$ sample is [C_4mpyr]-[$AlCl_4$] and gives rise to the bands at 347 and the 179 cm^{-1}.

The three remaining unassigned bands at 306, 264 and 259 cm^{-1} that increased in intensity upon increasing the $AlCl_3$ concentration in the C_4mpyrNTf$_2$/$AlCl_3$ system are also evident in the spectra of the C_4mpyrNTf$_2$/Al(NTf$_2$)$_3$ mixtures and the pure Al(NTf$_2$)$_3$. Hence, these bands are indicative of "Al^{3+} coordinated" NTf_2^- where the ligand is bidentate. In pure Al(NTf$_2$)$_3$, the 264 cm^{-1} band has a very small intensity and is only detected through curve fitting analysis, while in the C_4mpyrNTf$_2$/Al(NTf$_2$)$_3$ and the C_4mpyrNTf$_2$/$AlCl_3$ mixtures the 264 and 259 cm^{-1} bands are almost equivalent in intensity. Both bands therefore almost certainly originate from conformations of NTf_2^- coordinated to an Al^{3+} cation. Furthermore, the 259 cm^{-1} band is probably a strong indicator of bidentate NTf_2^- coordination to Al^{3+} via two oxygen atoms (O,O), as evidenced in the single crystal structure[61] and the theoretical calculations on the Al(NTf$_2$)$_3$ compound (see Figure 7c). The 264 cm^{-1} band is probably due to a different coordination mode as it is very weak in the spectrum of pure Al(NTf$_2$)$_3$ where O,O coordination of NTf_2^- is preferred. This is supported by the complex solution ^{27}Al NMR spectrum of Al(NTf$_2$)$_3$ which suggests more than one mode of NTf_2^- coordination.

During our investigation it came to our attention that the research groups of Endres and Krossing were concurrently conducting a similar speciation study to ours. Their investigation showed aluminium could not be electrodeposited from an Al(NTf$_2$)$_3$-saturated C_4mpyrNTf$_2$ solution.[66] Therefore the reducible aluminium species in the C_4mpyrNTf$_2$/$AlCl_3$ system must be an aluminium complex containing both Cl^- and NTf_2^- ligands. Their study of aluminium electrodeposition was demonstrated only from the lower phase of the C_4mpyrNTf$_2$/$AlCl_3$ system at $x_{AlCl_3}=0.50$. If we then conclude that the octahedral ^{27}Al resonance observed in this lower phase is due to Al(NTf$_2$)$_3$ or a similar NTf_2-rich aluminium complex which does not give rise to metallic aluminium electrodeposition upon applying a sufficiently negative constant potential then the electroactive aluminium species in this phase must be a tetrahedral species of the type $[AlCl_w(NTf_2)_y]^{z-}$, where w is more than likely greater than y.

Allowing the biphasic C_4mpyrNTf$_2$/$AlCl_3$ mixture at $x_{AlCl_3}=0.50$ to stand for a few hours at 60 °C, whilst the phases are in the liquid state, a precipitate appeared in the lower phase whose quantity increased with time. Unfortunately, the precipitate could not be isolated and characterised, but it is believed to be Al(NTf$_2$)$_3$ as a similar precipitate was observed in the C_2mimNTf$_2$/$AlCl_3$ system and characterised as Al(NTf$_2$)$_3$.[66] Spectroscopic analysis of the lower phase at $x_{AlCl_3}=0.50$ supports the presence of Al(NTf$_2$)$_3$. The ^{27}Al NMR spectrum showed an octahedral resonance with a similar chemical shift and linewidth to the octahedral ^{27}Al resonance in the spectrum of C_4mpyrNTf$_2$/Al(NTf$_2$)$_3$, and the ν_{expand} mode at 758 cm^{-1} and the two strong bands at 259 and 306 cm^{-1} in the Raman spectrum coincide with bands in the spectra of C_4mpyrNTf$_2$/Al(NTf$_2$)$_3$ and Al(NTf$_2$)$_3$ indicative of "Al^{3+} coordinated" NTF_2^- anions.

Since the reducible aluminium species in chloroaluminate melts is the chloro-bridged $Al_2Cl_7^-$ species, the existence of bridged aluminate species in the C_4mpyrNTf$_2$/$AlCl_3$ system, other than $Al_2Cl_7^-$, was also considered. To investigate this possibility, the Raman spectra of bridged aluminate species $Al_2Cl_6(NTf_2)^-$ and $Al_2Cl_5(NTf_2)_2^-$ were calculated. More detailed results are included in the Supporting Information (see Figure S3 and Tables S5 and S6). For these species, there was no Raman active mode of significant intensity that could be attributed to the vibrational motion of the Al-

Cl-Al or Al-NTf_2-Al bridges. Therefore we were not able to identify the presence of a bridge aluminium-containing species in the $C_4mpyrNTf_2/AlCl_3$ system.

Discussion and Conclusions

A DSC, theoretical, Raman and ^{27}Al NMR spectroscopic investigation of the room temperature ionic liquid $C_4mpyrNTf_2$ and its mixtures with $AlCl_3$ is reported here. The main objective of this work was to gain an insight into the type of aluminium-containing species generated in $C_4mpyrNTf_2/AlCl_3$ solutions and to endeavour to identify which species is ultimately responsible for aluminium electrodeposition from these solutions.

The ^{27}Al NMR data revealed the presence of both tetrahedrally and octahedrally coordinated aluminium species, with the former being more prominent. The octahedral resonance is probably due to NTf_2-rich aluminium-containing species such as $Al(NTf_2)_3$ or $[AlCl_2(NTf_2)_2]^-$. Depending on the composition of the $C_4mpyrNTf_2/AlCl_3$ mixture, the tetrahedral resonance can be due to either $AlCl_4^-$ or $[AlCl_w(NTf_2)_y]^{z-}$, where $w > y$ being the more likely scenario, or both. Theoretical calculations on prospective aluminium complexes showed that octahedral geometries are preferred when the complexes are NTf_2-rich and tetrahedral geometries are preferred when they are Cl-rich. In octahedral complexes the NTf_2^- ligand is bidentate as opposed to monodentate in tetrahedral complexes.

Valuable ionic association information of the NTf_2^- anion in $C_4mpyrNTf_2/AlCl_3$ mixtures can be gained by analysis of the bands in the Raman spectra. The band at 741 cm^{-1} is assigned to ν_{expand} in "free" NTf_2^- and refers to a complex mixture of internal coordinates such as ν_s(SNS), δ(SNS), $\delta(CF_3)$ and $\delta(SO_2)$ which make the entire NTf_2^- anion expand and contract. Bands at 746 and 758 cm^{-1} are assigned to ν_{expand} in "Al^{3+} coordinated" NTf_2^-. Theoretical calculations suggest the band at 746 cm^{-1} originates from NTf_2^- anions that are coordinated via an N atom (either monodentate or N,O bidentate coordination) whereas that at 758 cm^{-1} originates from NTf_2^- anions that are bidentate coordinated via O,O atoms. The latter was validated by examination of the Raman spectrum of pure $Al(NTf_2)_3$. This octahedral $Al(NTf_2)_3$ complex was synthesised directly and characterisation by ^{27}Al and ^{19}F NMR revealed the presence of several isomers, highlighting the versatile coordinating ability of the NTf_2^- anion. No evidence for bridged aluminium species was found.

At $x_{AlCl_3} = 0.50$, the $C_4mpyrNTf_2/AlCl_3$ mixture was biphasic and aluminium could only be electrodeposited from the lower turbid phase. The electroactive species involved was more than likely a tetrahedral complex of the type $[AlCl_w(NTf_2)_y]^{z-}$, where $w > y$. The upper clear phase was electrochemically inactive because it was shown to be $C_4mpyrAlCl_4$ and it is well known in chloroaluminate melts that $AlCl_4^-$ is not reducible to aluminium metal. It was also noted that the volume of the upper and lower phases at $x_{AlCl_3} = 0.50$ were approximately equivalent, which leads us to speculate that the following equilibrium may exist:

$$2\,C_4mpyrNTf_2 + 2\,AlCl_3 \rightleftharpoons C_4mpyrAlCl_4\ \text{(upper phase)} + C_4mpyrAlCl_2(NTf_2)_2\ \text{(lower phase)}$$

Since tetrahedral and octahedral aluminium species were both shown to exist in the lower phase by ^{27}Al NMR and that evidence for $Al(NTf_2)_3$ precipitation exists, the following equilibrium for the lower phase can therefore be envisaged:

$$2\,C_4mpyrAlCl_2(NTf_2)_2 \rightleftharpoons C_4mpyrCl + C_4mpyrAlCl_3(NTf_2) + Al(NTf_2)_{3(s)}$$

Hence, the reducible aluminium species in the lower phase may be narrowed to tetrahedral $[AlCl_3(NTf_2)]^-$ or octahedral $[AlCl_2(NTf_2)_2]^-$. The calculated binding energies for these aluminium species are summarised in Table 3.

Table 3. Calculated binding energies for selected aluminium species.

Species	Coordination	Binding energies [kJ mol^{-1}][a]
$AlCl_4^-$	–	5630.4
$Al_2Cl_7^-$	–	5538.2
$[AlCl_3(NTf_2)]^-$	N	5485.4
	O	5495.1
$[AlCl_2(NTf_2)_2]^-$	2×O,O	5379.5
	O,O + N,O	5360.5
	2×N	5341.3
	2×O	5339.2
	2×N,O	5343.1
	N + O	5340.5

[a] Per Al atom.

From the data it can be seen that the binding energy decreases as Cl^- anions are displaced by NTf_2^- anions in the inner coordination sphere of Al^{3+}, that is, the complex is destabilised. This would indicate that the reduction potential of the aluminium species might move to more positive values upon coordination by NTf_2^- anions. The binding energies of both $[AlCl_3(NTf_2)]^-$ and $[AlCl_2(NTf_2)_2]^-$ are lower than that of $AlCl_4^-$ and, more importantly, $Al_2Cl_7^-$. Since it is known that $Al_2Cl_7^-$ can be reduced to aluminium in chloroaluminate melts these findings indicate $[AlCl_3(NTf_2)]^-$ and $[AlCl_2(NTf_2)_2]^-$ may be reducible within the $C_4mpyrNTf_2$ window. Hence, the electroactive species involved here are probably $[AlCl_3(NTf_2)]^-$ or $[AlCl_2(NTf_2)_2]^-$.

Acknowledgements

E.I.I. gratefully acknowledge generous allocations of computing time from the National Facility of the Australian Partnership for Advanced Computing. The authors would like to thank Dr. Iko Burgar of CSIRO Materials Science and Engineering and Jo Cosgriff of CSIRO Molecular and Health Technologies for collecting the NMR and MS data, respectively, on the $Al(NTf_2)_3$ complex. Financial support for this work was pro-

vided by the Light Metals Flagship through its Flagship Collaboration Fund and by the ARC through the Centre of Excellence in Electromaterials Science. Fellowship support from the Australian Research Council for E.I.I. (Australian Postdoctoral Fellow), A.M.B. and D.R.M. (Federation Fellowships) is gratefully acknowledged.

[1] J. Robinson, R. A. Osteryoung, *J. Electrochem. Soc.* **1980**, *127*, 122–128.
[2] B. J. Welch, R. A. Osteryoung, *J. Electroanal. Chem.* **1981**, *118*, 455–466.
[3] H. L. Chum, R. A. Osteryoung, *Ionic Liquids* (Eds.: D. Inman, D. G. Lovering), Plenum Press, New York, N.Y., **1981**, 407–423.
[4] J. J. Auborn, Y. L. Barberio, *J. Electrochem. Soc.* **1985**, *132*, 598–601.
[5] S. D. Jones, G. E. Blomgren, *J. Electrochem. Soc.* **1989**, *136*, 424–427.
[6] R. T. Carlin, W. Crawford, M. Bersch, *J. Electrochem. Soc.* **1992**, *139*, 2720–2727.
[7] Q. Liao, W. R. Pitner, G. Stewart, C. L. Hussey, G. R. Stafford, *J. Electrochem. Soc.* **1997**, *144*, 936–943.
[8] Y. Zhao, T. J. VanderNoot, *Electrochim. Acta* **1997**, *42*, 3–13.
[9] Y. Zhao, T. J. VanderNoot, *Electrochim. Acta* **1997**, *42*, 1639–1643.
[10] C. A. Zell, F. Endres, W. Freyland, *Phys. Chem. Chem. Phys.* **1999**, *1*, 697–704.
[11] A. P. Abbott, C. A. Eardley, N. R. S. Farley, G. A. Griffith, A. Pratt, *J. Appl. Electrochem.* **2001**, *31*, 1345–1350.
[12] F. Endres, M. Bukowski, R. Hempelmann, H. Natter, *Angew. Chem.* **2003**, *115*, 3550–3552; *Angew. Chem. Int. Ed.* **2003**, *42*, 3428–3430.
[13] J. Lu, D. Dreisinger, *Ionic liquids as green solvents: Progress and prospects* (Eds.: R. D. Rogers, K. R. Seddon), ACS Symposium series 856, American Chemical Society, Washington, DC, **2003**, 495–508.
[14] M. Zhang, V. Kamavaram, R. G. Reddy, *J. Met.* **2003**, *55*, 54–57.
[15] V. Kamavaram, R. G. Reddy, *Metal Separation Technologies III*, Engineering Conferences International, Brooklyn, NY, **2004**, 143–151.
[16] T. Jiang, M. J. Chollier Brym, G. Dubé, A. Lasia, G. M. Brisard, *Surf. Coat. Technol.* **2006**, *201*, 1–9.
[17] T. Jiang, M. J. Chollier Brym, G. Dubé, A. Lasia, G. M. Brisard, *Surf. Coat. Technol.* **2006**, *201*, 10–18.
[18] T. A. Zawodzinski, R. A. Osteryoung, *Inorg. Chem.* **1987**, *26*, 2920–2922.
[19] T. A. Zawodzinski, R. A. Osteryoung, *Inorg. Chem.* **1990**, *29*, 2842–2847.
[20] A. K. Abdul-Sada, A. M. Greenway, K. R. Seddon, T. Welton, *Org. Mass Spectrom.* **1993**, *28*, 759–765.
[21] Q.-X. Qin, M. Skyllas-Kazacos, *J. Electroanal. Chem.* **1984**, *168*, 193–206.
[22] C. J. Smit, T. P. J. Peters, *Light Metals 1986* (Ed.: R. E. Miller), TMS, Warrendale, PA, **1986**, 253–260.
[23] P. K. Lai, M. Skyllas-Kazacos, *Electrochim. Acta* **1987**, *32*, 1443–1449.
[24] P. K. Lai, M. Skyllas-Kazacos, *J. Electroanal. Chem.* **1988**, *248*, 431–440.
[25] R. T. Carlin, R. A. Osteryoung, *J. Electrochem. Soc.* **1989**, *136*, 1409–1419.
[26] J. S. Wilkes, M. J. Zaworotko, *J. Chem. Soc. Chem. Commun.* **1992**, 965–967.
[27] N. Brausch, A. Metlen, P. Wasserscheid, *Chem. Commun.* **2004**, 1552–1553.
[28] S. Zein El Abedin, E. M. Moustafa, R. Hempelmann, H. Natter, F. Endres, *Electrochem. Commun.* **2005**, *7*, 1111–1116.
[29] S. Zein El Abedin, E. M. Moustafa, R. Hempelmann, H. Natter, F. Endres, *ChemPhysChem* **2006**, *7*, 1535–1543.
[30] M.-J. Deng, P.-Y. Chen, T.-I. Leong, I.-W. Sun, J.-K. Chang, W.-T. Tsai, *Electrochem. Commun.* **2008**, *10*, 213–216.
[31] L. Xue, C. W. Padgett, D. D. DesMarteau, W. T. Pennington, *Solid State Sci.* **2002**, *4*, 1535–1545.
[32] L. Xue, D. D. DesMarteau, W. T. Pennington, *Solid State Sci.* **2005**, *7*, 311–318.
[33] A.-V. Mudring, A. Babai, S. Arenz, R. Giernoth, *Angew. Chem.* **2005**, *117*, 5621–5624; *Angew. Chem. Int. Ed.* **2005**, *44*, 5485–5488.
[34] a) A. Babai, A.-V. Mudring, *Dalton Trans.* **2006**, *1828*–1830; b) S.-F. Tang, A. Babai, A.-V. Mudring, *Angew. Chem.* **2008**, *120*, 7743–7746; *Angew. Chem. Int. Ed.* **2008**, *47*, 7631–7634.
[35] a) A. Babai, A.-V. Mudring, *Inorg. Chem.* **2006**, *45*, 3249–3255; b) A. Babai, A.-V. Mudring, *Z. Anorg. Allg. Chem.* **2008**, *634*, 938.
[36] K. Mikami, O. Kotera, Y. Motoyama, H. Sakaguchi, M. Maruta, *Synlett* **1996**, 171–172.
[37] M. Baak, W. Bonrath, H. Pauling, WO98/21197, **1998**.
[38] M. Earle, B. J. MCauley, A. Ramani, K. R. Seddon, J. M. Thomson, WO02/072260 A2, **2002**.
[39] T. Katase, T. Onishi, S. Imashuku, K. Murase, T. Hirato, Y. Awakura, *Electrochemistry* **2005**, *73*, 686–691.
[40] M. B. Boxer, H. Yamamoto, *Org. Lett.* **2005**, *7*, 3127–3129.
[41] P. Johansson, S. P. Gejji, J. Tegenfeldt, J. Lindgren, *Electrochim. Acta* **1998**, *43*, 1375–1379.
[42] Gaussian 03 (Revision C.02), M. J. Frisch, G. W. Trucks, H. B. Schlegel, G. E. Scuseria, M. A. Robb, J. R. Cheeseman, J. A. Montgomery, Jr., T. Vreven, K. N. Kudin, J. C. Burant, J. M. Millam, S. S. Iyengar, J. Tomasi, V. Barone, B. Mennucci, M. Cossi, G. Scalmani, N. Rega, G. A. Petersson, H. Nakatsuji, M. Hada, M. Ehara, K. Toyota, R. Fukuda, J. Hasegawa, M. Ishida, T. Nakajima, Y. Honda, O. Kitao, H. Nakai, M. Klene, X. Li, J. E. Knox, H. P. Hratchian, J. B. Cross, V. Bakken, C. Adamo, J. Jaramillo, R. Gomperts, R. E. Stratmann, O. Yazyev, A. J. Austin, R. Cammi, C. Pomelli, J. W. Ochterski, P. Y. Ayala, K. Morokuma, G. A. Voth, P. Salvador, J. J. Dannenberg, V. G. Zakrzewski, S. Dapprich, A. D. Daniels, M. C. Strain, O. Farkas, D. K. Malick, A. D. Rabuck, K. Raghavachari, J. B. Foresman, J. V. Ortiz, Q. Cui, A. G. Baboul, S. Clifford, J. Cioslowski, B. B. Stefanov, G. Liu, A. Liashenko, P. Piskorz, I. Komaromi, R. L. Martin, D. J. Fox, T. Keith, M. A. Al-Laham, C. Y. Peng, A. Nanayakkara, M. Challacombe, P. M. W. Gill, B. Johnson, W. Chen, M. W. Wong, C. Gonzalez, J. A. Pople, Gaussian, Inc., Wallingford CT, **2004**.
[43] A. P. Scott, L. Radom, *J. Phys. Chem.* **1996**, *100*, 16502–16513.
[44] J. Timmermans, *J. Phys. Chem. Solids* **1961**, *18*, 1–8.
[45] J. L. Gray, G. E. Maciel, *J. Am. Chem. Soc.* **1981**, *103*, 7147–7151.
[46] J. S. Wilkes, J. S. Frye, G. F. Reynolds, *Inorg. Chem.* **1983**, *22*, 3870–3872.
[47] S. Takahashi, M.-L. Saboungi, R. J. Klinger, M. J. Chen, J. W. Rathke, *J. Chem. Soc. Faraday Trans.* **1993**, *89*, 3591–3595.
[48] K. Ichikawa, T. Matsumoto, *J. Magn. Reson.* **1985**, *63*, 445–453.
[49] K. Ichikawa, T. Jin, T. Matsumoto, *J. Chem. Soc. Faraday Trans. 1* **1989**, 175–185.
[50] L. J. Hardwick, M. Holzapfel, A. Wokaun, P. Novak, *J. Raman Spectrosc.* **2007**, *38*, 110–112.
[51] M. Herstedt, M. Smirnov, P. Johansson, M. Chami, J. Grondin, L. Servant, J. C. Lassegues, *J. Raman Spectrosc.* **2005**, *36*, 762–770.
[52] I. Rey, P. Johansson, J. Lindgren, J. C. Lassegues, J. Grondin, L. Servant, *J. Phys. Chem. A* **1998**, *102*, 3249–3258.
[53] M. Castriota, T. Caruso, R. G. Agostino, E. Cazzanelli, W. A. Henderson, S. Passerini, *J. Phys. Chem. A* **2005**, *109*, 92–96.
[54] D. Brouillette, D. E. Irish, N. J. Taylor, G. Perron, M. Odziemkowski, J. E. Desnoyers, *Phys. Chem. Chem. Phys.* **2002**, *4*, 6063–6071.
[55] Z. Wang, W. Gao, X. Huang, Y. Mo, L. Chen, *J. Raman Spectrosc.* **2001**, *32*, 900–905.
[56] K. Fujii, V. Fujimori, T. Takamuku, R. Kanzaki, Y. Umebayashi, S.-I. Ishiguro, *J. Phys. Chem. B* **2006**, *110*, 8179–8183.
[57] M. Herstedt, W. A. Henderson, M. Smirnov, L. Ducasse, L. Servant, D. Talaga, J. C. Lassegues, *J. Mol. Struct.* **2006**, *783*, 145–156.
[58] W. A. Henderson, M. Herstedt, V. G. Young, Jr., S. Passerini, H. C. De Long, P. C. Trulove, *Inorg. Chem.* **2006**, *45*, 1412–1414.
[59] B. Klassen, R. Aroca, G. A. Nazri, *J. Phys. Chem.* **1996**, *100*, 9334–9338.
[60] S. Takahashi, L. A. Curtiss, D. Gosztola, N. Koura, M.-L. Saboungi, *Inorg. Chem.* **1995**, *34*, 2990–2993.
[61] P. Schulz, Crystal structure of the $Al(NTf_2)_3$ compound, unpublished results.

[62] H. A. Øye, M. Jagtoyen, T. Oksefjell, J. S. Wilkes, *Mater. Sci. Forum* **1991**, *73*, 183–190.
[63] R. J. Gale, B. Gilbert, R. A. Osteryoung, *Inorg. Chem.* **1978**, *17*, 2728–2729.
[64] R. J. Gale, R. A. Osteryoung, *Inorg. Chem.* **1980**, *19*, 2240–2242.
[65] B. Gilbert, H. Olivier-Bourbigou, F. Favre, *Oil and Gas Science and Technology-Rev. IFP* **2007**, *62*, 745–759.
[66] P. Eide, Q. Liu, S. Zein El Abedin, F. Endres, I. Krossing, *Eur. J. Org. Chem.* in press.

Received: August 8, 2008
Published online: January 8, 2009

